ELSEVIER

Progress in Biophysics & Molecular Biology 85 (2004) 451–472

Progress in Biophysics & Molecular Biology

www.elsevier.com/locate/pbiomolbio

Towards whole-organ modelling of tumour growth

T. Alarcón[a,*,1], H.M. Byrne[b], P.K. Maini[a]

[a] *Centre for Mathematical Biology, Mathematical Institute, University of Oxford, 24-29 St Giles', Oxford OX1 3LB, UK*
[b] *Centre for Mathematical Medicine, Division of Applied Mathematics, School of Mathematical Sciences, University of Nottingham, Nottingham NG7 2RD, UK*

Abstract

Multiscale approaches to modelling biological phenomena are growing rapidly. We present here some recent results on the formulation of a theoretical framework which can be developed into a fully integrative model for cancer growth. The model takes account of vascular adaptation and cell-cycle dynamics. We explore the effects of spatial inhomogeneity induced by the blood flow through the vascular network and of the possible effects of p27 on the cell cycle. We show how the model may be used to investigate the efficiency of drug-delivery protocols.

Keywords: Cancer; Vascular networks; Blood flow heterogeneity; Cell cycle; p27

1. Introduction

Cancer is reckoned to be responsible for one in every five deaths in the Western world (Alberts et al., 1994). It is therefore a major killer in the developed countries. All the diseases under this heading are characterised by profound disturbances of the most fundamental rules of behaviour of the cell in a multicellular organism. In spite of the enormous resources dedicated to investigate this disease, many of the current treatments are not entirely effective. The systematic approach used in mathematical modelling, guiding experiments by clinicians and biologists, might help to elucidate the fundamental mechanisms underlying the progression of the disease and lead to either improved or entirely new therapeutic strategies.

While modelling tumour growth is one of the most active areas of research within the Mathematical and Theoretical Biology community, much work remains to be done in order to

*Corresponding author. Department of Computer Science, University College London, Gower Street, London WC1E 6BT, UK. Tel.: +44-20-7679-3701; fax: +44-20-7387-1397.

E-mail address: t.alarcon@cs.ucl.ac.uk (T. Alarcón).

[1] Dedicate this paper to Joseph Edmund Byrne who was born while the paper was being written.

0079-6107/$ - see front matter © 2004 Elsevier Ltd. All rights reserved.
doi:10.1016/j.pbiomolbio.2004.02.004

produce clinically relevant and predictive models. One obstacle that must be overcome is the intrinsic multiple scale nature of tumour growth. It involves processes occurring over a variety of time and length scales: from the tissue scale (for example, vascular re-modelling) to intra-cellular processes (for example, progression through the cell cycle of both normal and cancer cells).

Most existing models focus on one scale. Whilst this may provide valuable insight into processes occurring at that scale, it does not address the fundamental problem of how phenomena at different scales are coupled. In this article, we review recent research we have carried out with the aim of eventually formulating a multiple scale model of tumour growth capable of integrating a hierarchy of processes occurring at different scales, the so-called Physiome approach.

The paper is organised as follows. In Section 2, we briefly review the current literature on mathematical models of tumour growth. Section 3 contains a summary of our cellular automaton model for tumour growth. This model, which addresses the issue of how an inhomogeneous distribution of nutrients affects growth, is highly phenomenological. In particular it assumes that all cells divide synchronously. In Section 4, we propose a mathematical model for the effects of extracellular nutrient levels (in particular oxygen) on the cell division cycle, with a view to combining this model with the one presented in Section 3. An indication of how this can be done and the kind of results one might expect is given in Section 5. There we summarise recent work on cancer chemotherapy, using a model that couples vascular adaptation, colony growth and cell-cycle kinetics (Ribba et al., 2003). Finally, in Section 6 we summarise our results and perspectives for future research.

2. Review of current models

Here, we briefly review some of the approaches that have been used to model tumour growth. Broadly speaking, we can divide these into two approaches: continuum models, mathematically formulated in terms of partial differential equations (PDEs), and cellular automaton (CA) models. Our aim in this section is to give a flavour of the different approaches used by researchers in this field; an exhaustive and complete review of existing models is beyond the scope of this paper. For more extensive reviews see, for example, Alber et al. (2002), Moreira and Deutsch (2002) and Preziosi (2003).

2.1. Continuum models

We will start by briefly reviewing the different continuum models. We give here a rough classification of the approaches that have been used to investigate different aspects of tumour growth and include references to works that we believe are representative.

Some of the earliest mathematical models of tumour growth are due to Greenspan (Greenspan, 1972a, b). His models of avascular tumour growth were formulated as moving boundary problems, in which the solid tumour grows in suspension. The models do not allow for cellular heterogeneity within the tumour mass and the treatment of the mechanical properties of the tissue is rather basic. For extensions of Greenspan's moving boundary formulation see Adam (1987a, b), Byrne and Chaplain (1997) and McElwain and Morris (1978).

Significant progress was made with the introduction of multiphase models. These models extend the moving boundary approach to incorporate cellular heterogeneity and the use of more complex mechanical laws to describe the response of the tissue to external forces. Multiphase models have now been used to model avascular growth (Byrne et al., 2003; Please et al., 1998; Ward and King, 1997, 1999), vascular growth (Breward et al., 2003), ductal carcinoma in situ (Franks et al., 2003) and tumour encapsulation (Jackson and Byrne, 2002).

The approaches described above draw upon methods from fluid and continuum mechanics. Models based on different approaches have been successful in describing other aspects of tumour growth. One approach involves using reaction-diffusion theory as a modelling framework. Such models have been used to describe invasion and different aspects of tumour-induced angiogenesis (Chaplain, 1996; Levine et al., 2001; Marchant et al., 2001; Orme and Chaplain, 1996). An alternative approach which has been used to model interactions between tumour growth and the immune system is based on kinetic theory and Boltzmann-like equations (Bellomo and Preziosi, 2000).

For a more extensive review of continuum modelling of tumour growth see Preziosi (2003).

2.2. Cellular automaton models

Whereas continuum models describe cell populations by means of continuous fields, CA deal with the dynamics of discrete elements.[2] These elements take their state from a discrete (finite) space of states and evolve in discrete space and time. The dynamics of the elements is given in terms of local rules (either deterministic or probabilistic). Some of the models we describe below introduce modifications to the classical definition of a CA. In particular, some of them introduce diffusive substances (such as nutrients or signalling cues) which are described by means of continuum fields. These models are categorised as hybrid CAs and are the basis for the development of the multiple scale models we will discuss in Sections 3–5.

We review below four CA models that have been proposed to describe four aspects of tumour growth, namely, avascular growth, vascular growth, invasion and angiogenesis.

The model proposed by Dormann and Deutsch (2002) reproduces the layer structure observed in avascular tumour colonies cultured as spheroids (Folkman and Hochberg, 1973). Dormann and Deutsch (2002) formulated a two-dimensional CA model, actually a lattice-gas model (see Rothman and Zalesky, 1997), which reproduces many of the features observed experimentally. One of the key features of their model is the inclusion of a chemotactic substance released by necrotic cells. Necrotic cells accumulate in the centre of the spheroid where the nutrient is very scarce. The necrotic signal was introduced in order to reproduce the effects of cell flow towards the centre of the spheroid observed by Dorie et al. (1982, 1986). This flow is necessary in order to obtain the growth saturation characteristic of multicellular spheroids.[3]

In Patel et al. (2001), a CA model of tumour growth in the presence of native vasculature was proposed[4] to analyse the role of host vascular density and tumour metabolism on tumour growth.

[2] In the biological context these elements might be either individual cells or (small) clusters of them.

[3] This saturation has been achieved in continuum models of avascular tumour growth.

[4] Although neither interaction between colony development and vasculature nor angiogenesis is not taken into account.

Tumour cells are known to survive severe hypoxic stress due to their ability to switch to anaerobic (glycolytic) metabolism as the major source of cellular energy. This, in turn, increases the environmental acidity. Several results regarding the interplay between vessel density, increased acidity, and tumour progression are obtained. Probably the most significant of them is the presence of a sharp transition between states of initial tumour confinement and efficient invasiveness when H^+ production passes through a critical value. This has been observed in experiments (Gatenby and Gawlinsky, 1996). The models formulated by Dormann and Deutsch (2002) and Patel et al. (2001) are both hybrid CA models.

Turner and Sherrat (2002) studied malignant invasion using the extended Potts model (Graner and Glazier, 1992). They investigate how malignant cell phenotypes, in particular adhesion properties, affect cancer invasiveness. Their extended Potts model is based on the minimisation of an energy function by a Monte Carlo method. Each (biological) cell occupies several sites of the lattice. The energy function includes a term for surface energy depending on cell-to-cell and cell-to-extracellular matrix adhesion forces, a mechanical energy term accounting for elastic deformation and cell growth, and haptotaxis. The model can be simulated to investigate how the maximum depth of invasion changes as different parameters relating to cell-to-cell and cell-to-extracellular matrix adhesion and haptotaxis are varied.

A CA model for angiogenesis based on endothelial cell migration in response to gradients of tumour angiogenic factor (TAF) (chemotaxis) and fibronectin[5] (haptotaxis) has been proposed by Anderson and Chaplain (1998). In this model vessel tip migration is modelled by a biased random walk. The corresponding transition probabilities depend on the local concentrations of TAF and fibronectin and are derived from finite-difference discretisations of macroscopic level partial differential equations (PDEs). Additional rules are provided for branching and anastomosis.[6] The results can reproduce experimental observations on solid tumour implants in the cornea of animals (Anderson and Chaplain, 1998).

For more extensive reviews of CA modelling of biological systems in general and tumour growth in particular see Alber et al. (2002) and Moreira and Deutsch (2002), respectively.

3. Tumour growth in an inhomogeneous environment

Our first step towards a multiscale, integrative model of tumour growth is to couple cell growth to the (complex) environmental conditions. In particular, we have formulated a model to analyse the effect of blood flow and oxygen heterogeneity on tumour growth (Alarcón et al., 2003a). In this section, we briefly introduce our model and summarise our main results.

Despite the highly organised structure of blood vessels in normal tissue, as compared to the *chaotic* organisation of vascular beds in cancer tissue (Baish et al., 1996), the blood flow distribution in normal tissue is, for a number of reasons, strongly inhomogeneous. Firstly, blood is a complex suspension of different elements, with a complex rheology (Pries et al., 1994). Secondly, it is not a network of rigid tubes but a structure which interacts with the flow and

[5] Fibronectin is a molecule that enhances cell adhesion to the extracellular matrix. It is a component of the extracellular matrix and is also expressed by the endothelial cells.

[6] Anastomosis is the formation of a loop by fusion of two capillaries.

remodels itself accordingly (Pries et al., 1998). Additionally, *haematocrit*, i.e. the fraction of the total volume of blood occupied by red blood cells, is not distributed at bifurcations in the same way as blood flow (Fung, 1993). Consequently, the distribution of oxygen in the vascular network is highly irregular. In Alarcón et al. (2003a) we developed a CA model which allows us to study how these phenomena affect the growth of cellular colonies and the malignant invasion of healthy tissue. Initially, we simulated blood and haematocrit (i.e. oxygen) flow through a regular network of blood vessels. We then accounted for blood rheology and adaptation of the vascular network. This enabled us to determine the haematocrit distribution within the vessels. The next step involved coupling this model with a hybrid cellular automaton model that described the dynamics of the surrounding tissue.

3.1. Blood flow simulations: structural adaptation and complex blood rheology

We now describe the main elements of our blood flow simulations. Two main effects we take into account are vascular structural adaptation and blood rheology.

Guided by experiments involving vascular beds (Pries et al., 1995) and the fact that the vascular system continually adapts to the demands of the surrounding tissue,[7] Pries and co-workers formulated an adaptation mechanism which describes how the lumen radius of a given vessel, $R(t)$, is modified by these effects (Pries et al., 1998):

$$R(t+\Delta t) = R(t) + R\Delta t\left(\log\left(\frac{\tau_w}{\tau(P)}\right) + k_m \log\left(\frac{\dot{Q}_{ref}}{\dot{Q}H} + 1\right) - k_s\right). \quad (1)$$

In (1) Δt is the time scale, $\dot{Q}$ is the flow rate, $\dot{Q}_{ref}$, k_m and k_s are constants described below, H is the haematocrit, $\tau_w = R\Delta P/L$ is the wall shear stress acting on a vessel of length L. P is the transmural pressure, and $\tau(P)$ the magnitude of the corresponding "set point" value of the wall shear stress (see Pries et al., 1998; Alarcón et al., 2003a for details). The expression for $\tau(P)$ that we use was obtained by fitting to data from the rat mesentery (Pries et al., 1998):

$$\tau(P) = 100 - 86[\exp(-5000\log(\log P))]^{5.4}. \quad (2)$$

The second term on the right-hand side of Eq. (1), i.e. the difference between the logarithms of the wall shear stress and its corresponding *set point* value, represents the response to mechanical or haemodynamic stimuli. It is proposed (Pries et al., 1995) that vascular networks adapt themselves in order to maintain a fixed relationship (given in Eq. (2)) between transmural pressure and wall shear stress. Equally, structural adaptation of vascular beds also occurs in response to the metabolic demands of the surrounding tissue. Consequently, if the flow in some vessels drops and the tissue becomes poorly supplied with oxygen or other metabolites, then the vasculature will be stimulated to grow. This phenomenon is accounted for by the third term in the right-hand side of Eq. (1). We remark that the metabolic stimulus is always positive and increases with decreasing red blood cell flux, $\dot{Q}H$. The constant k_m indicates how rapidly the vasculature adapts to the metabolic needs of the tissue. The constant k_s represents the so-called *shrinking tendency* and accounts for the need for growth factors to maintain or increase the size of a given vessel.

[7] This implies that network morphology is not only determined by genetic information but also by physical mechanisms that act locally in response to mechanical, metabolic and biochemical stimuli.

Blood is a complex suspension of cells and molecules of a wide range of sizes. Thus, modelling blood as a Newtonian fluid is a very crude approximation. Consider blood flowing through a tube of radius R and suppose that the volume fraction occupied by the red blood cells (RBCs) (i.e. the haematocrit) is H. For a given value of H, the viscosity of the blood depends non-monotonically on R and three different flow regimes may be identified. If R is much greater than the typical size of a red blood cell, the viscosity is independent of R. As R decreases the viscosity decreases (the Fahraeus–Lindqvist effect) until the vessel radius is of the order of 15–20 μm. This behaviour of the viscosity has its origin in the behaviour of the RBCs. The shear stress (SS) profile in a vessel is inhomogeneous: the SS is larger next to the tube and diminishes as we move towards the axis. This profile leads to migration of the RBCs towards the low SS regions (i.e. towards the axis) that yields a layer of plasma next to the wall. This larger fraction of periphery plasma then produces a lower effective viscosity. The viscosity then attains a minimum and, thereafter, increases as R decreases (Pries et al., 1994). In our simulations we follow Pries et al. (1994) and take the following expression for the viscosity as a function of R and H:

$$\mu = \mu_{\text{plasma}}\left[1 + (\mu^*_{0.45} - 1)\frac{(1-H)^C - 1}{(1-0.45)^C - 1}\left(\frac{2R}{2R-1.1}\right)^2\right]\left(\frac{2R}{2R-1.1}\right)^2,$$

$$\mu^*_{0.45} = 6e^{-0.17R} + 3.2 - 2.44e^{-0.06(2R)^{0.645}},$$

$$C = (0.8 + e^{-0.15R})\left(-1 + \frac{1}{1 + 10^{-11}(2R)^{12}}\right) + \frac{1}{1 + 10^{-11}(2R)^{12}}. \tag{3}$$

In Eqs. (3) μ_{plasma} is the viscosity of the plasma which we assume constant ($\mu_{\text{plasma}} = 5$ cP).

Since μ depends on H, the haematocrit distribution is an important factor when determining the hydrodynamic state of the network. The simplest way to proceed is to assume that at each bifurcation the distribution of H depends on the flow velocity in each of the daughter vessels (Fung, 1993). Roughly speaking, a larger proportion of the haematocrit from the parent vessel is transported along the faster branch. Additionally, it has been observed in model experiments with RBC-like shaped pellets that at bifurcations where the ratio between the velocities of the branches exceeds a certain threshold, all the haematocrit enters the faster branch. Combining these results, we assume that, at a bifurcation, the haematocrit is distributed between the two daughter vessels as follows (see Fig. 1 for definitions):

$$\begin{aligned} &H_p = H_1 + H_2, \\ &\frac{H_1}{H_2} = \alpha\frac{v_1}{v_2} \quad \text{if } \frac{v_1}{v_2} < \text{THR}, \\ &H_1 = H_p \quad \text{if } \frac{v_1}{v_2} > \text{THR}. \end{aligned} \tag{4}$$

In Eq. (4) $v_i \equiv \dot{Q}_i/\pi R_i^2$ is the average flow velocity in a cross-section orthogonal to the axis of the vessel, α is a phenomenological parameter which accounts for the strength of the asymmetry of the haematocrit distribution at bifurcations, and THR is the critical ratio of the velocities of the branches above which all the haematocrit goes to the faster branch. In our simulations we have used $\alpha = 0.5$ and $\text{THR} = 2.5$ that were taken from experiments reported in (Fung, 1993). The aforementioned effect of accumulation of the RBCs around the axis of the vessels also contribute

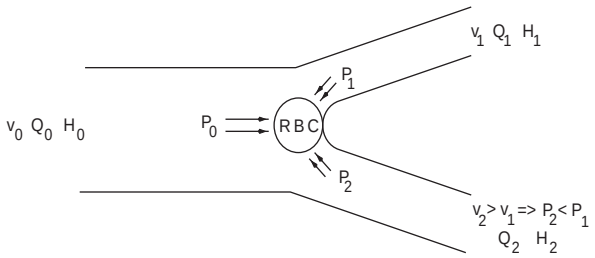

Fig. 1. Schematic representation of a bifurcation in the vascular network, illustrating the mechanism that gives rise to uneven haematocrit distribution. RBC stands for red blood cell. See text for details.

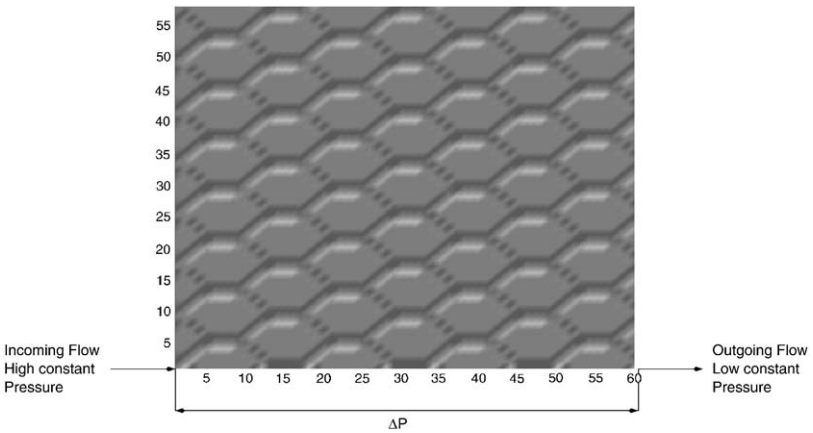

Fig. 2. Initial conditions for the adaptation algorithm: all vessels have the same radius (10 μm) and length (80 μm). In the blood flow simulations, we have imposed no-flux conditions for all the vessels on the boundary of the domain except at the ends marked in the figure as "incoming flow" and "outlet flow", where a given value of the current has been prescribed (see Alarcón et al., 2003a for further details). In all the figures hereafter, the numbers on the axis refer to the position in the cellular automaton lattice which is a subset of $\mathbb{Z}^2$. One unit in this lattice corresponds to 20 μm in real tissue.

to the uneven distribution of haematocrit at bifurcations. This effect is even more important when a big vessel bifurcates into a very small daughter vessel and a much bigger one, and has been observed in real vascular networks as well as in model experiments.

We have carried out numerical simulations starting with a hexagonal network where all the vessels have the same initial radii (see Fig. 2) and assuming Poiseuille's flow, we have used Kirchoff's law to calculate all the hydrodynamical quantities, and Eq. (4) to obtain the haematocrit distribution. The radii are then updated using Eq. (2). The process is repeated until a stationary state is reached. Typical results, presented in Fig. 3, illustrate the highly heterogeneous distribution of haematocrit obtained across the network.

Fig. 4 shows results concerning the relative importance of the different factors taken into account (complex blood rheology and vascular structural adaptation) on producing the distribution of haematocrit shown in Fig. 3. Comparing Figs. 4(a) and (b), we see that the structural adaptation mechanism yields a more branched pattern (Fig. 4(b)) whereas complex blood rheology (i.e. the Fahraeus–Lindqvist effect) distributes more evenly the haematocrit. Thus,

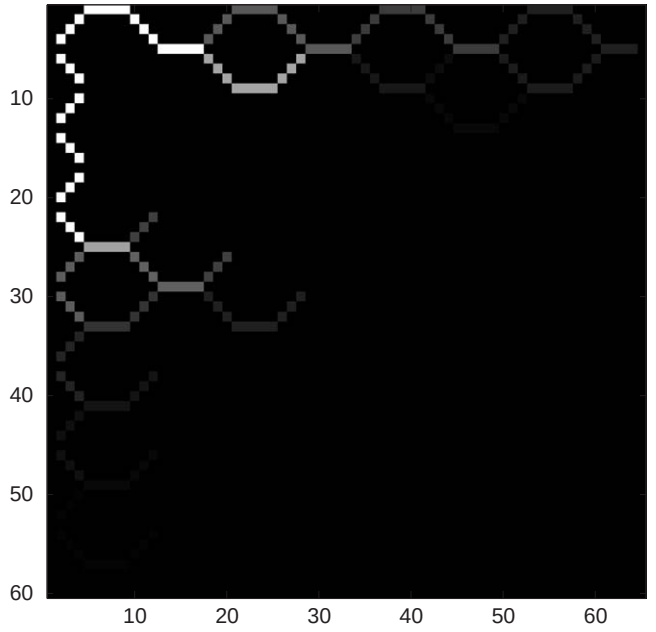

Fig. 3. Distribution of haematocrit obtained from our blood flow simulations (in grey scale: lighter corresponds to higher haematocrit, darker to lower haematocrit). The haematocrit is defined as the ratio between the volume occupied by the RBCs and the total volume of blood and it is therefore a non-dimensional quantity.

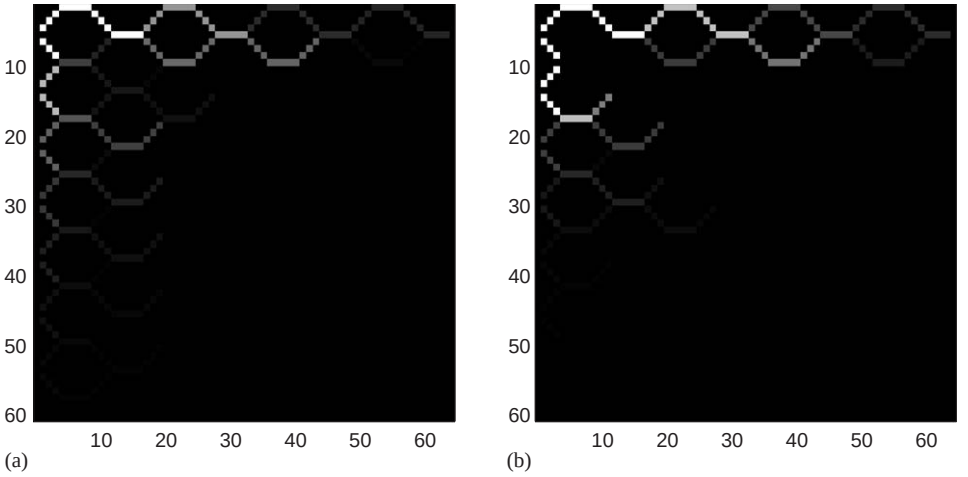

Fig. 4. These two plots show the distribution of haematocrit (in grey scale: lighter corresponds higher haematocrit, darker to lower haematocrit) for two different cases. In (a) the structural adaptation algorithm is not acting (the vessels have constant radii (10 μm)) and the viscosity is given by Eq. (3). In (b), the structural adaptation mechanism is at work but the blood viscosity is constant over the network ($\mu = 5$ cP).

we can conclude that the major contribution to the non-uniformity of the haematocrit distribution comes from the structural adaptation mechanism, although, the geometry of the vascular network is also important in determining the haematocrit distribution.

3.2. Cell dynamics

Having determined the haematocrit (i.e. oxygen distribution) associated with the vascular network shown in Fig. 2, we now investigate how a colony of cells evolves in response to the associated distribution of oxygen in the tissue. The dynamics of the cell colony is modelled using a hybrid cellular automaton. Our two-dimensional model consists of an array of $N \times N$ automaton elements,[8] which will eventually be identified with real cells. The state of each element is defined by a state vector, whose components correspond to features of interest. For now, the state vector has three components: (i) occupation status, i.e. whether an element is occupied by a normal cell, a cancer cell, an empty space or a vessel, (ii) cell status, i.e. whether the cell is in a proliferative or a quiescent state, and (iii) the local oxygen concentration. The state vector evolves according to prescribed local rules which update a given element from its own state and that of its neighbours' on the previous time step (see Alarcón et al., 2003a for full details). In the present case, we consider a simple square lattice, so that each cell has four (nearest) neighbours. While we view cells as discrete entities, the oxygen concentration is treated as a continuous field, as the typical length of an oxygen molecule is very small compared to the characteristic size of a cell. The time evolution of the oxygen concentration is governed by a reaction-diffusion equation, with sinks, sources and boundary conditions determined by the corresponding distribution of cells and vessels in the host tissue. Since the characteristic relaxation time of the oxygen distribution is much smaller than the time scale corresponding to the tissue, we apply the adiabatic approximation, whereby the oxygen distribution is in equilibrium with the cell colony.

The rules of the automaton are inspired by generic features of tumour growth, such as the ability of cancer cells to elude the control (or feedback) mechanisms which maintain stasis in normal tissues. They can also alter their local environment, providing themselves with better conditions for growth and, eventually, for invasion of the host organism (King, 1996). This phenomenon is implemented in our simulations by allowing the cancer cells to survive under lower levels of oxygen than normal cells. In practice, cancer cells exhibit a remarkable ability to endure very low levels of oxygen. A well-known, but not exclusive, characteristic of cancer cells is their ability under hypoxic conditions to enter a quiescent state, in which they suspend all activity, including any cell division that is not essential for survival (Royds et al., 1998). They can remain in this latent state for a certain period of time, before starving to death. In addition, these cells may express growth factors that stimulate angiogenesis. Finally, we incorporate into our model competition between cancer and normal cells for the existing resources (nutrients, metabolites, etc.), as proposed by Gatenby (1996). Normal tissue is a non-competitive cell community, since, under conditions such as overcrowding or starvation, feedback mechanisms act to maintain tissue stasis. However, when members of this community become cancerous, a new population, with its own dynamics, is formed. For further progression of the transformed population to occur, the tumour cells must compete for space and resources with the normal cells. For details of the actual rules of our automaton we refer the reader to Alarcón et al. (2003a).

In Alarcón et al. (2003a) by suitable choice of the initial condition we studied growth and invasion, in each case comparing, in turn, the impact of a homogeneous and a heterogeneous

[8] In our simulations we have taken $N = 61$ square elements. Each of these elements represents an area of Δ^2 with $\Delta = 20$ μm, which corresponds roughly to the area occupied by one cell. We are thus simulating a total area of 1.2 mm^2.

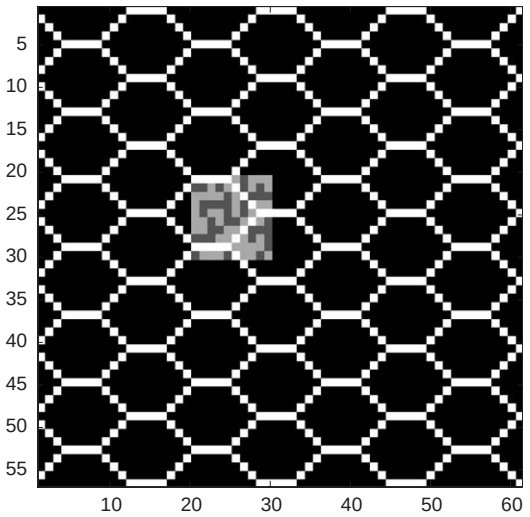

Fig. 5. Initial conditions for our CA model. Black spaces are empty elements, dark grey are occupied by cancer cells, light grey are occupied by normal cells, and white by vessels.

supply of oxygen from the supporting vasculature[9] on the ability of the tumour cells to dominate the normal tissue. The initial conditions for growth are given in Fig. 5. For brevity, this is only the case we will discuss here. Whereas for the homogeneous environment we observe an isotropic pattern of growth (Figs. 6(e) and (d)), for the heterogeneous environment we observe a highly irregular growth pattern, since the colony grows preferentially into regions where the oxygen concentration is higher (see Fig. 7). Figs. 6(c) and (f) show how the number of cancer cells evolves over time for the inhomogeneous and homogeneous environments, respectively. We note that in the inhomogeneous case the colony saturates at a maximal size whereas in the homogeneous case the colony grows until all the available space is occupied. This behaviour can be explained as follows. If a cell divides and the new cell is situated in a poorly oxygenated region, this cell dies within a few iterations of our automaton. Consequently, all viable cells are located in well-oxygenated regions of the domain (Fig. 7(a)). While the regions in which the cells are accumulating are rich in oxygen, the amount of oxygen being supplied is finite and can only sustain a certain number of cells. The combination of these two effects leads to the stationary patterns observed in Figs. 6(a) and (b). On the contrary, in a homogeneous environment there are now no poorly oxygenated regions, so the colony is free to grow isotropically, until it occupies all the space available.

Hence, our model predicts that environmental inhomogeneity restricts dramatically the ability of malignant colonies to grow and invade healthy tissue. This is because non-uniform oxygen perfusion leads to the existence of very poorly oxygenated regions which the cancer cells fail to populate: any cells that reach these regions starve after a few iterations.

[9] We have used two distributions of haematocrit across the vasculature. For the heterogeneous case we have used the haematocrit distribution shown in Fig. 3. For the homogeneous case, we have simply distributed the same total amount of haematocrit homogeneously throughout the network.

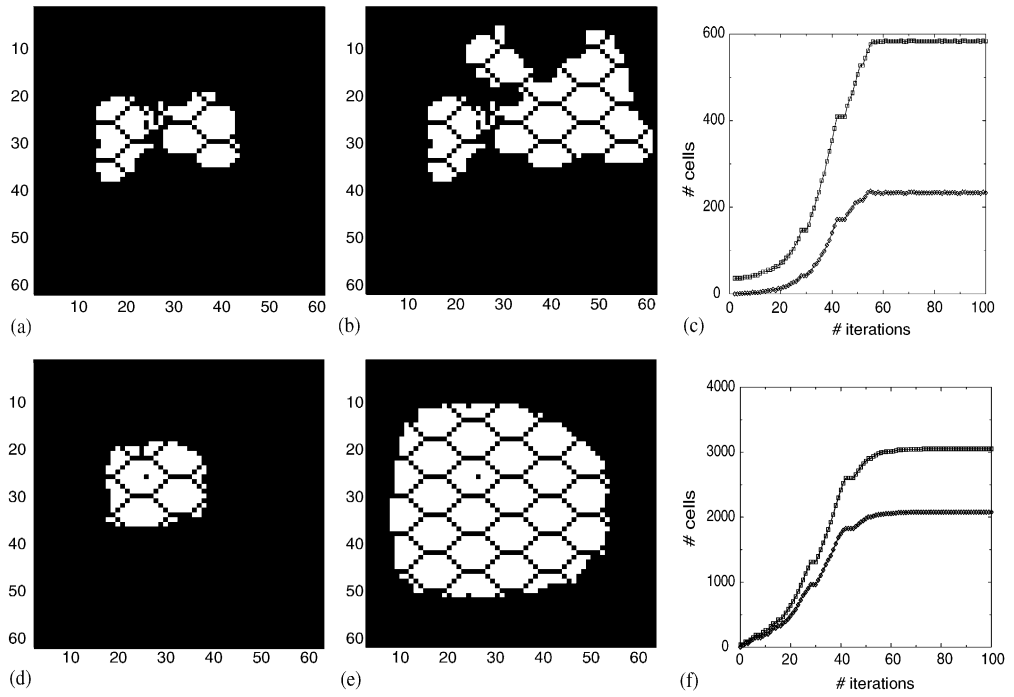

Fig. 6. Series of images showing the evolution of the spatial distribution of cells for growth in inhomogeneous (panels a and b), and homogeneous environments (panels d and e). In panels (a), (b), (d), and (e) white spaces are occupied by cancer cells, whereas black spaces are either empty or occupied by vessels. Panels (c) and (f) show the time evolution of the number of (cancer) cells for the heterogeneous and homogeneous cases, respectively. Squares represent the total number of cancer cells (proliferating + quiescent). Diamonds correspond to the quiescent population. In both cases, normal cells are taken over after a few iterations and therefore do not appear in these figures.

Our model has several shortcomings. First, intracellular processes such as cell division and apoptosis are included on a purely phenomenological basis. In Section 4, we introduce a model that allows for more accurate description of the biochemical mechanisms involved. Equally, we have not included any feedback between cell growth and vascular adaptation: the vasculature remains static whereas the colony develops. In Section 5, we explain how it may be possible to modify our model to allow for feedback from the cell dynamics to the structural adaptation mechanism.

4. Cell-cycle dynamics: effects of hypoxia

In the CA model described in Section 3, cell division is incorporated in a purely phenomenological way: at each time step, if the oxygen concentration is high enough, cells divide. Otherwise the cell either dies (normal cells) or becomes quiescent (cancer cells). In practice, cell division is governed by a well orchestrated sequence of events that takes place inside the cell: the cell cycle. The rate of progression through the cell cycle depends on, among other factors, the availability of nutrients, in particular oxygen (Alberts et al., 1994). Our aim in this section is to

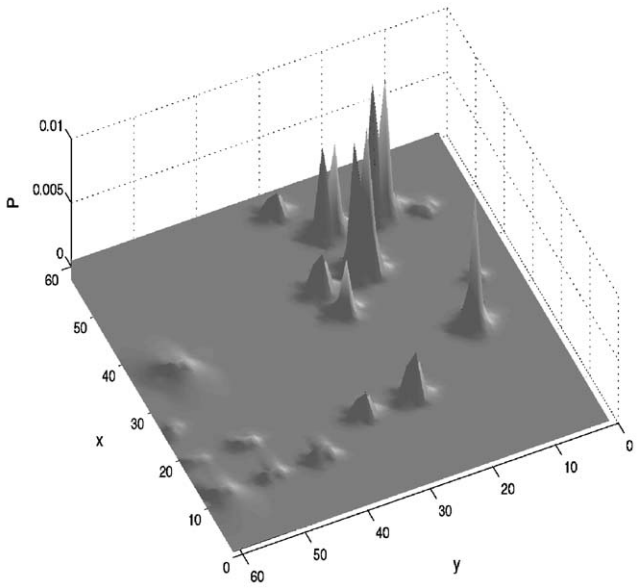

Fig. 7. Stationary distribution of oxygen.

summarise a mathematical model we have proposed to describe the effect of extracellular oxygen on the cell cycle (Alarcón et al., 2003b). In so doing, we take a further step towards constructing a multiscale model by linking the intracellular biochemical processes (in this case, the cell cycle) to the extracellular distribution of nutrient.

The cell cycle is usually divided into four phases: G_1, S, G_2, and M. In G_1 (G = gap), the cell is not committed to division and the chromosomes do not replicate. Replication of nuclear DNA occurs during the S phase. Completion of mitosis occurs in the final phase, M. The interval between DNA replication and division is the so-called G_2 phase. Both G_1 and G_2 allow the cell additional time for growth. The cell also passes through two irreversible transitions. The first transition occurs at the end of G_1 and is called "Start" (see Fig. 8 for a schematic representation). During G_1 the cell monitors its environment and size. When the external conditions and the size of the cell are suitable, the cell commits itself to DNA synthesis and division. This transition is irreversible: once the cell enters the S phase and DNA replication commences, division has to be completed. The second transition, "Finish", occurs when DNA replication is completed. Once the cell has checked that DNA and chromatide alignment have occurred, the Finish transition is triggered and the cell finally divides into two daughter cells.

Modelling the cell cycle is immensely complex so we try to obtain some insight by considering the simpler case of the yeast cell. It is important to keep this in mind when interpreting our results. The events occurring during the cell cycle are controlled by a series of molecular signals. The central components of this network are two families of proteins: the cyclin-dependent kinases (CDKs) and the cyclins (Funk, 1999). The CDKs induce downstream processes by phosphorylating selected proteins. However, to do this, they must be activated by binding to the cyclins. Cyclins are so-called because they undergo a cycle of synthesis and degradation

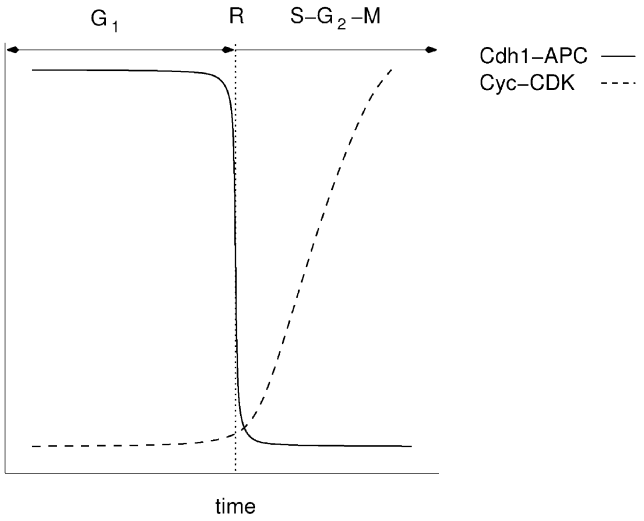

Fig. 8. Schematic representation of the dynamics of the cell-cycle. The dotted line represents the restriction point (R) at which the "Start" transition occurs. Before the cell goes through this transition, it is in the G_1 stage. After the "Start" transition the cell enters the S phase in which DNA synthesis takes place. See text for details.

parallel to the cell division cycle. While the CDK network is very complex, here we consider only its essential features (Tyson and Novak, 2001).

During G_1, CDK activity is low because the relevant cyclin partners are missing: their production is inhibited and they are rapidly degraded. At "Start" cyclin synthesis is promoted, and hence the CDKs are activated. CDK activity remains high during S, G_2, and M, since it is necessary for DNA replication and other processes occurring during the final stages of the cycle. At "Finish", Cdh1 is activated. When active, these two proteins present the target proteins (CDKs) to the proteolytic machinery of the cell for degradation. Together, they label cyclins for destruction at the end of the cycle, allowing the control system to return to G_1. In turn, the cyclin-CDK complexes inhibit Cdh1 (see Tyson and Novak, 2001 for a more detailed discussion).

It is well known that the dynamics of the cell cycle can be affected by environmental conditions, such as the level of extracellular oxygen, with low oxygen concentration (hypoxia) altering progression through the cell division cycle (Gardner et al., 2001). The response of the G_1/S transition to hypoxia is mediated by the protein p27, an element of the CDK network whose production is upregulated under hypoxia (Funk, 1999; Gardner et al., 2001). p27 mediates hypoxia-induced arrest of the G_1/S transition by inhibiting Cyc-CDK complex formation and, thereby, inhibiting DNA synthesis (Fig. 9).

The regulation of the cell cycle in normal and cancer cells exhibits remarkable differences (Funk, 1999). One of the most important differences is how the two cell populations respond to hypoxia: whereas most normal cells undergo apoptosis when the hypoxic stress is too intense or persists for too long, cancer cells appear to have a much higher resistance to hypoxia than their normal counterparts. This resistance is (in part) due to their ability to enter into a quiescent state under severe or prolonged hypoxic stress (Royds et al., 1998). Of course, if the levels of oxygen become extremely low or hypoxia lasts for a very long time, the cancer cells eventually die. We will

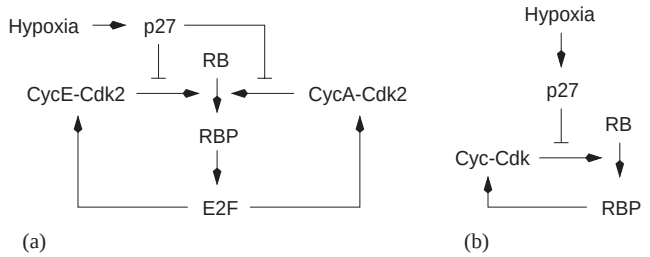

Fig. 9. Schematic representation of the mechanism for hypoxia-induced arrest of G_1/S phase: (a) represents the original mechanism proposed by Gardner et al. (2001) and (b) corresponds to our simplified version for modelling purposes. In scenario (a), RBP (which stands for the phosphorylated form of the retinoblastoma (RB) protein) production is activated by the complexes CycE-Cdk2 and CycA-Cdk2. A high concentration of RBP is essential for DNA synthesis since it activates the E2F transcription factor, which regulates many of the genes involved in the initiation of the S phase, basically through activation of the Cyc-CDK complexes. Hypoxia activates the production of p27, which, in turn, inhibits the activity of the Cyc-CDK complexes, thus delaying the initiation of the S phase. We consider a simplified version for modelling purposes (b), in which only one type of Cyc-CDK complex is considered and RBP is assumed to directly activate this complex.

be using two terms, hypoxia-induced arrest and hypoxia-induced quiescence, that must be properly defined. Hypoxia-induced arrest refers to a situation in which the transition through G_1/S is delayed by the low level of oxygen. However, eventually the cell will go through it. Hypoxia-induced quiescence, on the contrary, implies a dramatic change in the dynamics: the transition through the G_1/S transition is not simply delayed but the system actually loses the ability to undergo that transition. Hence, whereas arrest leads to an increase in the length of the cell cycle, quiescence implies complete disruption to the cell cycle. Mathematically, this difference is related to whether a bifurcation in the cell-cycle control system exists (Alarcón et al., 2003b). One might find odd the fact that stopping proliferation gives an advantage to the cancer cells over the normal cells. The solution to this apparent paradox is the following. Normal cells, when submitted to a long period of hypoxia (i.e. prolonged arrest), undergo hypoxia-induced apoptosis. On the contrary, quiescent cancer cells do not undergo hypoxia-induced apoptosis[10] (Royds et al., 1998). When normal cells die by starvation, more oxygen becomes available. This increasing in the oxygen concentration is detected by quiescent cancer cells, which then return to their normal progression through the cell cycle. This is the mechanism cancer cells use to obtain an advantage over normal cells.

Although the role played by p27 in normal and cancer cells is the same, its rates of expression differ so that the concentration of p27 is, generally, smaller in cancer cells than in normal cells (Bai et al., 2001; Funk, 1999; Philipp-Staheli et al., 2001). It has also been observed that normal cells in the presence of growth factors exhibit reduced levels of p27 (Leshem and Halevy, 2002; Saito et al., 2001). In spite of these differences, mutations in the chromosome encoding for p27 are scarcely found in human cancer (Funk, 1999). Hence, it is likely that the different behaviour of p27 in normal and cancer cells is produced by different mechanisms controlling the rates of expression of p27.

[10] However, if the hypoxic stress lasts for too long quiescent cancer cells undergo necrosis.

Tyson and Novak (2001) claim that regulation of the cell cycle is due to the creation and destruction of stable steady states of the molecular regulatory system of the cell division process. In Alarcón et al. (2003b) we extended the model proposed by Tyson and Novak (2001) to account for the impact of hypoxia on G_1/S transition (Gardner et al., 2001). Our model can be written in dimensionless form as

$$\frac{dx}{d\tau} = \frac{(1 + b_3 u)(a_4 - x)}{J_3 + a_4 - x} - \frac{b_4 m x y}{J_4 + x}, \tag{5}$$

$$\frac{dy}{d\tau} = a_4 - (a_1 + a_2 x + a_3 z) y, \tag{6}$$

$$\frac{dm}{d\tau} = \eta m \left(1 - \frac{m}{m_*}\right), \tag{7}$$

$$\frac{dz}{d\tau} = \chi(m) - c_2 \frac{P}{B + P} z, \tag{8}$$

$$\frac{du}{d\tau} = d_1 - (d_2 + d_1 y) u, \tag{9}$$

where $x = [\text{Cdh1}]$, $y = [\text{Cyc}]$, m is the mass of the cell, $z = [\text{p27}]$, u is the concentration of non-phosphorylated retinoblastoma protein and P is the oxygen tension. In Eq. (8), the production rate for the p27 protein, $\chi(m)$, depends on the type of cell we are considering:

$$\chi(m) = \begin{cases} c_1 & \text{for a cancer cell,} \\ c_1 \left(1 - \dfrac{m}{m_*}\right) & \text{for a normal cell.} \end{cases} \tag{10}$$

The justification for our definitions of $\chi(m)$ come from experimental observations which show that stimulating growth downregulates p27 in normal cells (Leshem and Halevy, 2002; Saito et al., 2001), but such stimulation has no effect on cancer cells (Dhillon and Mudryj, 2002; Park et al., 2001).

A detailed analytical and numerical study of the model equations (5)–(9) is presented in Alarcón et al. (2003b). Here, we simply state three key results:

- Reducing the oxygen tension prolongs the duration of G_1 in the normal cell-cycle model. Furthermore, a reduction in the oxygen tension by a factor 1/40–1/50 increases the duration of G_1 by 20–25%. This means that in a large population of (identical) cells, approximately 20–25% more cells will be in G_1 phase. A similar increase was observed in experiments by Gardner et al. (2001).
- For our cancer cell-cycle model, the period of division increases as the oxygen tension decreases (see Fig. 10). However, this increase does not continue indefinitely: for very low oxygen tensions the model predicts that hypoxia causes the cell cycle to stop, as indicated by the vertical asymptote we find in the division period (see Alarcón et al., 2003b). This is consistent with the observed transition of cancer cells to quiescence under hypoxia (Folkman and Hochberg, 1973). Our normal cell-cycle model does not exhibit hypoxia-induced quiescence.

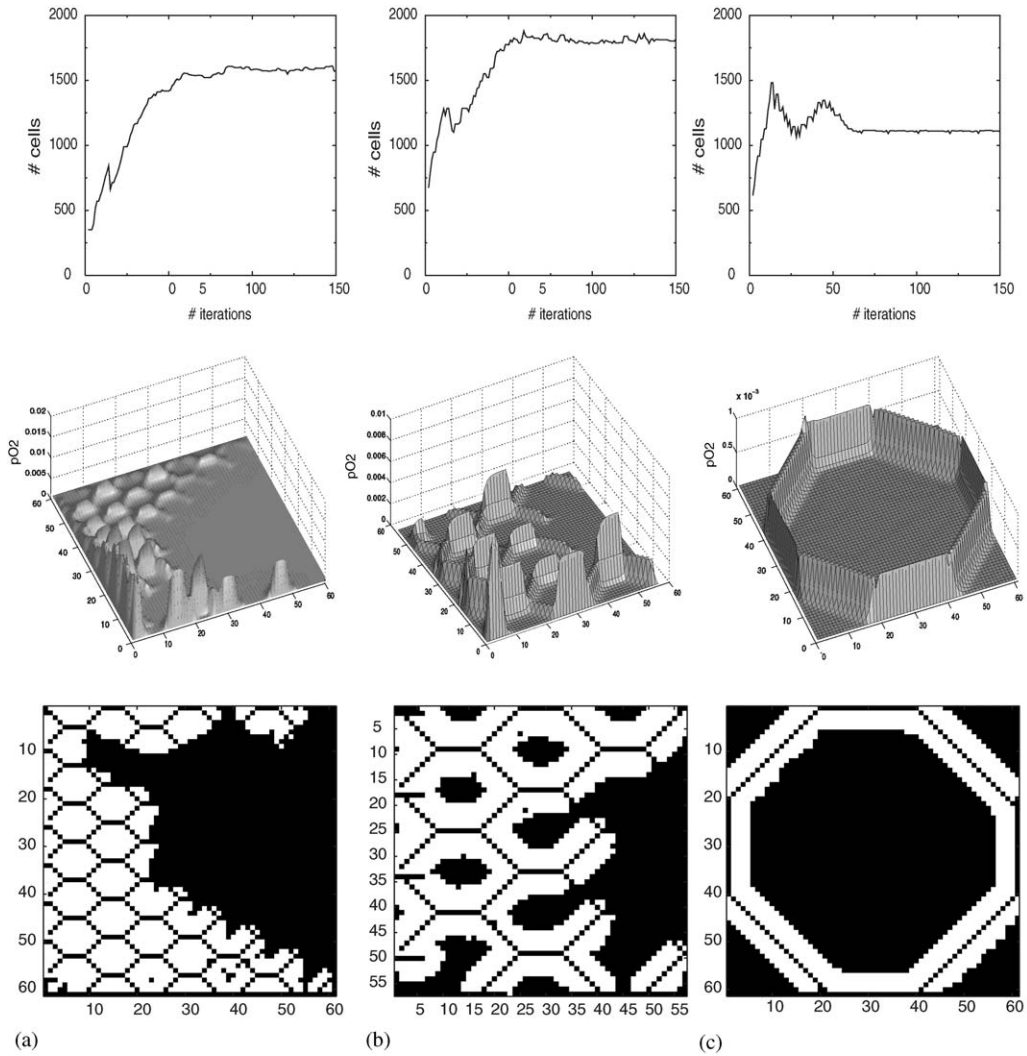

Fig. 10. Simulation for systems whose vascular networks have different sparsity, i.e. we have varied the *vascular density*, defined as the number of vessels per surface unit. In column (a) we have plotted the results for a system with vascular density = 114 vessels/mm^2, column (b) corresponds to vascular density = 24 vessels/mm^2, and column (c) corresponds to vascular density = 4 vessels/mm^2. The results plotted in the first row corresponds to the evolution of the size of cancer colony in time (where each iteration corresponds to 15 h, which is an estimation of the duplication time of our cancer cells), the second row, to the stationary distribution of oxygen (pO_2 in dimensionless units), and the third row, to the stationary cell distribution. In the middle set of figures, the vertical axis is the oxygen concentration. In the bottom panel of each column white spaces are occupied by cancer cells, whereas black spaces are either empty or occupied by vessels.

Thus, our models reproduce this important difference between the behaviour of normal and cancer cells under hypoxia.

- The predicted proliferation rate of our cancer cell-cycle model is higher than that of the normal cell-cycle model. This is a characteristic feature of most types of cancer (Alberts et al., 1994).

5. Application: lymphoma chemotherapy efficiency

In this section, we review an application of this modelling approach to determine the efficiency of the chemotherapy regime usually given to patients with non-Hodgkin's lymphoma (full details can be found in Ribba et al., 2003). This example serves a two-fold purpose: to show how our model can be used to model cancer therapy and assess its efficiency, and also as an example of how to incorporate cell-cycle dynamics and the interaction between cell dynamics and vascular adaptation.

Non-Hodgkin's lymphomas (NHL), which appear on lymph nodes, exhibit a remarkable ability to metastasise, thus posing a difficult problem to clinicians. NHL patients are currently treated with CHOP chemotherapy, which is a combination of drugs of which Doxorubicin is the most active (Lepage et al., 1993). CHOP is usually administered over a total of 6–8 cycles separated by 21 day intervals (Couderc et al., 2000). Our aim is to analyse the efficiency of CHOP chemotherapy in terms of this dosing interval.

The basic theoretical framework used in Ribba et al. (2003) to investigate this problem is a modified version of the model presented in Section 3. First, we have included a blood-borne drug (Doxorubicin) which is transported to the tumour by the circulation and then diffuses into the tissue. The local concentration of (extracellular) drug is found by solving the appropriate boundary value problem. Drug activity is modelled by means of the appropriate pharmacokinetics, describing how the concentration of drug in plasma decays with time, and pharmacodynamics, providing the survival probability of a cell for a given (local) drug concentration. Concerning Doxorubicin pharmakokinetics, we use the so-called one-compartment model, i.e.

$$\frac{\mathrm{d}C_\mathrm{b}}{\mathrm{d}t} = -kC_\mathrm{b}, \tag{11}$$

$$C_\mathrm{b}(0) = \frac{\text{dose}}{V_\mathrm{d}}, \tag{12}$$

where C_b is the concentration of drug in plasma, V_d is volume distribution of the drug and k is the decay rate of drug, which is related to Doxorubicin half-life time, $t_{1/2}$, by $k = \ln 2/t_{1/2}$.[11] The model we are using for Doxorubicin pharmacodynamics prescribes a survival probability, y, given by (see Hardman et al., 2001):

$$y = a + \frac{1}{b + k_\mathrm{d}C}, \tag{13}$$

where C is the (local) drug concentration and a, b, and k_d are positive constants.[12]

Also included is a simple cell-cycle model in which the duration of each phase of the cell cycle is fixed according to various NHL-kinetic studies (Brons et al., 1992; Erlanson et al., 1995; Stokke et al., 1998). An *age* is then assigned to each cell which is increased at each iteration and in this way the cells progress through the different stages of the cell-cycle (an ODE-based model like the one explained in Section 4 was not considered, although it could be included to improve the

[11] Pharmacodynamics parameter values: $V_\mathrm{d} = 682\ \mathrm{L\,m^{-2}}$, $t_{1/2} = 26$ h (Hardman et al., 2001).

[12] Pharmacokinetics parameter values: $a = 5 \times 10^{-3}$, $b = 1.005$ and $k_\mathrm{d} = 2.603\ \mathrm{cm^3/mg}$ (Hardman et al., 2001). a and b are non-dimensional.

model). Normal progression through the cell cycle may be disrupted by lack of nutrient, leading to quiescence or cell death, or cells may be killed by the drug.

Another important modification is that in this case the colony of cells can influence vascular morphology. Normal vasculature is known to be well organised and endowed with smooth muscle cells and pericytes. This allows the vessels to adapt their structure (Pries et al., 1998). Due to neovascularisation, cancer vessels are immature and therefore lack such structure. Consequently, they are not able to undergo structural adaptation. Furthermore cancer cells can destabilise established, mature vasculature, rendering it immature (Yancopoulos et al., 2000). Therefore, in the model of Ribba et al. whenever a vessel is engulfed by lymphoma cells it is assumed that it loses its ability for adaptation and its radius is fixed at random. Vessels not surrounded by lymphoma cells remain under the action of the structural adaptation mechanism Eq. (1). The status of all vessels (mature and immature) is updated at each time step.

The results of the simulations carried out in Ribba et al. (2003) indicate that the present clinical treatment is inefficient: NHL displayed significant population regrowth following each drug application. In some cases, by the end of the drug cycle the cell colony will manage to recover to a population exceeding that prior to drug administration. These results imply that the usual 21 day interval between cycles is too long for efficiently treating NHL. However, to improve efficiency, it is not enough to simply reduce the dosing interval; the interval must be reduced to a point at which additional drug cycles are applied before the unstable stage (i.e. the stage at which the tumour starts growing again) (Ribba et al., 2003).

The heterogeneity of blood flow appears to be a key contributing factor to these model observations. Simulations show that regrowth of the colony after Doxorubicin injection can be divided into two stages: a rapid and regular growth (first stage regrowth) until aggregation of cells leads to a large proportion of vessels becoming immature and thus structurally unstable. This structural instability leads to an extremely heterogeneous blood flow profile, causing consecutive regions to become hypoxic, and stimulating significant oscillations in lymphoma population size (second stage regrowth) (Ribba et al., 2003).

6. Conclusions

We have shown how, by answering specific, biologically meaningful questions, we are progressing towards a theoretical framework which encompasses an integrative approach to tumour growth. We are using the hybrid cellular automaton as a basic theoretical framework to combine models that couple scales ranging from the tissue scale (e.g. vascular structural adaptation) through to the intracellular scale (e.g. cell cycle). This has enabled us to tackle questions such as the effect on tumour growth of blood flow heterogeneity (Alarcón et al., 2003a) and the efficiency of current chemotherapy protocols for the treatment of non-Hodgkin's lymphomas (Ribba et al., 2003).

To our knowledge, this is the first attempt at a whole organ model for cancer. In our modelling framework, intercellular processes are represented by ordinary differential equations, extracellular processes by partial differential equations and cell processes by rules in a cellular automaton. Presently, the model is highly phenomenological and simple, with many processes not included. However, the over-arching framework presented here allows these aspects to be improved.

A major problem facing any vertical integration model is that if one simply takes a detailed model at one level and feeds it into the next vertical level, the number of equations increases exponentially and one simply replaces a biological system which one cannot understand by a computational model which one cannot understand and which is only an approximation. Therefore, at each horizontal level it is vital that, after understanding the detail, one devises caricature models which abstract the key phenomena. An example of this is the cell-cycle model in which we concentrated on a simple version of the very detailed models developed by Tyson and Novak, and through it were able to incorporate the effects of p27. This "module" can now be slotted into the overall vertical model framework. Of course, it is vital also to ensure that the vertical model, with these caricaturized horizontal levels, does not lead to spurious results as a consequence of these simplications, so the model must be tested for robustness. There is still a *long* way to go.

In cancer modelling we are at a much more primitive stage than in other Physiome projects (such as the heart). Therefore, the model we present here is somewhat generic and to validate it requires us to apply it to a particular cancer for which detailed data exists (such as colon cancer). We are presently beginning such a study.

As an example of possible future applications of our model, we present in Fig. 10 some results concerning the effect of varying the vessel density.[13] Comparing Fig. 10(a) and (b), we note that an increase in the stationary size of the colony is obtained when the *vascular density* (i.e. the number of vessels per mm^2) diminishes. Furthermore, the formation of cords (accumulations of cells around the vessels) is observed. As the vascular density diminishes, so does the haematocrit heterogeneity across the network. The subsequent homogenisation of the oxygen distribution yields the observed increase in the population. Cords form because, as the vasculature is sparser, there are regions which the oxygen cannot reach. However, if we diminish further the vascular density (Fig. 10(c)), we observe that the stationary population falls below the value of the case with higher vascular density (Fig. 10(a)). Moreover, in this case the haematocrit is homogeneously distributed. This result might be important for issues such as transport of blood-borne drugs: finding a balance between vascular density and blood flow heterogeneity could lead to an *optimal* drug supply.

To summarise, we have established a modelling framework with which we can eventually develop a realistic, multiple scale model of tumour growth. At present, our models are still largely phenomenological. However, filling these gaps is just one aspect of the work that must be done. As more detail is incorporated their computational implementation and analysis become more difficult. Developing appropriate numerical and analytical techniques will play a key role in efficiently implementing, understanding and exploiting these models.

Acknowledgements

TA thanks the EU Research Training Network (5th Framework): "Using mathematical modelling and computer simulation to improve cancer therapy" for funding this research. HMB

[13] The results shown in Fig. 10 correspond to our model with the cell-cycle kinetics and interaction with vascular adaptation introduced in Ribba et al. (2003).

thanks the EPSRC for funding as an Advanced Research Fellow. This paper is based on a talk given by PKM at the meeting: Modelling Cellular Function. He thanks Nic Smith for the invitation. This research (PKM) was supported in part by the National Science Foundation under Grant No. PHY99-07949. PKM would like to thank KITP, UC Santa Barbara for their kind hospitality.

References

Adam, J.A., 1987a. A mathematical model of tumour growth II: effects of geometry and spatial uniformity on stability. Math. Biosci. 86, 183–211.

Adam, J.A., 1987b. A mathematical model of tumour growth III: comparison with experiment. Math. Biosci. 86, 213–227.

Alarcón, T., Byrne, H.M., Maini, P.K., 2003a. A cellular automaton model for tumour growth in inhomogeneous environment. J. Theor. Biol. 225, 257–274.

Alarcón, T., Byrne, H.M., Maini, P.K., 2003b. A mathematical model of the effects of hypoxia on the cell-cycle of normal and cancer cells. J. Theor. Biol., submitted for publication.

Alber, M.S., Kiskowski, M.A., Glazier, J.A., Yi Jiang, 2002. On cellular automaton approaches to modeling biological cells. In: Rosenthal, J., Gilliam, G.S. (Eds.), Mathematical systems theory in Biology, Communication, and Finance, IMA, Vol. 142. Springer, New York, pp. 1–40.

Alberts, B., et al., 1994. Molecular Biology of the Cell, 3rd Edition. Garland Publishing, New York.

Anderson, A.R.A., Chaplain, M.A.J., 1998. Continuous and discrete mathematical models of tumor-induced angiogenesis. Bull. Math. Biol. 60, 857–899.

Bai, M.N.J., Agnantis, A., Skyrlas, E., Tsanou, S., Kamina, V., Galani, V., Kanavaros, P., 2001. Low expression of p27 protein combined with altered p53 and Rb/p16 expression status is associated with increased expression of cyclin A and cyclin B1 in diffuse B-cell lymphoma. Mod. Pathol. 14, 1105–1113.

Baish, J.W., Gazit, Y., Berk, D.A., Nozue, M., Baxter, L.T., Jain, R.K., 1996. Role of tumour architecture in nutrient and drug delivery: an invasion percolation-based model. Microvasc. Res. 51, 327–346.

Bellomo, N., Preziosi, L., 2000. Modelling and mathematical problems related to tumour evolution and its interaction with the immune system. 32, 413–452.

Breward, C.J.W., Byrne, H.M., Lewis, C.E., 2003. A multiphase model describing vascular tumour growth. Bull. Math. Biol. 65, 609–640.

Brons, P.P.T., Raemaekers, J.M.M., Bogman, M.J.J.T., van Erp, P.E.J., Boezeman, J.B.M., Pennings, A.H.M., Wessels, H.M.C., Haanen, C., 1992. Cell cycle kinetics in malignant lymphoma studied with in vivo iodeoxyuridine administration, nuclear Ki-67 staining, and flow cytometry. Blood 80, 2336–2343.

Byrne, H.M., Chaplain, M.A.J., 1997. Free boundary value problems associated with the growth and development of multicellular spheroids. Eur. J. Appl. Math. 8, 639–658.

Byrne, H.M., King, J.R., McElwain, D.L.S., 2003. A two-phase model of solid tumour growth. Appl. Math. Lett. 16, 567–573.

Chaplain, M.A.J., 1996. Avascular growth, anigiogenesis and vascular growth in solid tumours: the mathematical modelling of the stages of tumour development. Math. Comp. Model 23, 47–87.

Couderc, B., Dujols, J.P., Mokhtari, F., Norkowski, J.L., Slawinski, J.C., Schlaifer, D., 2000. The management of adult aggressive non-Hodgkin's lymphomas. Crit. Rev. Oncol. Hematol. 35, 33–48.

Dhillon, N.K., Mudryj, M., 2002. Ectopic expression of cyclin E in estrogen responsive cell abrogates antiestrogeb mediated growth arrest. Oncogene 21, 4626–4634.

Dorie, M.J., Kallman, R.F., Rapacchieta, D.F., Vanantwerp, D., Huang, Y.G., 1982. Migration and internalisation of cells and polysterene microspheres in tumour cell spheroids. Exp. Cell Res. 141, 201–209.

Dorie, M.J., Kallman, R.F., Coyne, M.A., 1986. Effect of cytochalasin B, nocodazole and irradiation on migration and internalisation of cells and polysterene microspheres in tumour cell spheroids. Exp. Cell Res. 166, 370–378.

Dormann, S., Deutsch, A., 2002. Modelling of self-organised tumour growth with a hybrid cellular automaton. Silico Biol. 2, 0035.

Erlanson, M., Lindh, J., Zackrison, B., Landberg, G., Roos, G., 1995. Cell kinetic analysis of non-Hodgkin's lymphomas using in vivo iodeoxyuridine incorporation and flow cytometry. Hematol. Oncol. 13, 207–217.

Folkman, J., Hochberg, M., 1973. Self-regulation of growth in three dimensions. J. Exp. Med. 138, 745–753.

Franks, S.J., Byrne, H.M., King, J.R., Lewis, C.E., 2003. Modelling the growth of ductal carcinoma in situ. J. Math. Biol., to appear.

Fung, Y.C., 1993. Biomechanics. Springer, New York.

Funk, J.O., 1999. Cancer cell cycle control. Anticancer Res. 19, 4772–4780.

Hardman, J.G., Limbird, L.E., Gilman, A.G., 2001. The Pharmacological Basis of Therapies. McGraw-Hill, New York.

Gatenby, R.A., 1996. Application of competition theory to tumour growth: implications for tumour biology and treatment. Eur. J. Cancer 32A, 722–726.

Gatenby, R.A., Gawlinsky, E.T., 1996. A reaction-diffusion model of cancer invasion. Cancer Res. 56, 5745–5753.

Gardner, L.B., Li, Q., Park, M.S., Flanagan, W.M., Semenza, G.L., Dang, C.V., 2001. Hypoxia inhibits G_1/S transition through regulation of p27 expression. J. Biol. Chem. 276, 7919–7926.

Graner, F., Glazier, J.A., 1992. Simulation of biological cell sorting using a two-dimensional extended Potts model. Phys. Rev. Lett. 69, 2013–2016.

Greenspan, H.P., 1972a. Models for the growth of a solid tumour by diffusion. Stud. Math. Appl. 51, 317–340.

Greenspan, H.P., 1972b. On the growth and stability of cell cultures and solid tumours. J. Theor. Biol. 56, 229–242.

Jackson, T., Byrne, H.M., 2002. A mathematical model of tumour encapsulation. Math. Biosci. 180, 307–328.

King, R.J.B., 1996. Cancer Biology. Longman, Harlow.

Lepage, E., Gisselbrecht, C., Haioun, C., Sebban, C., Tilly, H., Bosly, A., Morel, P., Herbrecht, R., Reyes, F., Coiffier, B., 1993. Prognostic significance of received relative dose intensity in non-Hodgkin's lymphoma patients: application to LNH-87 protocol. The GELA. (Groupe d'Etude des Lymphomes de l'Adulte.) Ann. Oncol. 651–656.

Leshem, Y., Halevy, O., 2002. Phosphorylation of pRb is required for HGF-induced muscle cell proliferation and is p27(kip1)-dependent. J. Cell Physiol. 191, 173–182.

Levine, H.A., Pamuk, S., Sleeman, B.D., Nilsen-Hamilton, M., 2001. Mathematical modeling of capillary formation and development in tumor angiogenesis: penetration into the stroma. Bull. Math. Biol. 63, 801–863.

Marchant, B.P., Norbury, J., Sherratt, J.A., 2001. Travelling wave solutions to a haptotaxis-dominated model of malignant invasion. Nonlinearity 14, 1653–1671.

McElwain, D.L.S., Morris, L.E., 1978. Apoptosis as a volume loss mechanism in mathematical models of tumour growth. Math. Biosci. 39, 147–157.

Moreira, J., Deutsch, A., 2002. Cellular automaton models of tumour development: a critical review. Adv. Complex Syst. 5, 247–267.

Orme, M.E., Chaplain, M.A.J., 1996. A mathematical model of vascular tumour growth and invasion. Math. Comput. Model. 23, 43–60.

Patel, A.A., Gawlinski, E.T., Lemieux, S.K., Gatenby, R.A., 2001. A cellular automaton model of early tumour growth and invasion: the effects of native tissue vascularity and increased anaerobic metabolism. J. Theor. Biol. 213, 315–331.

Park, C., Lee, I., Kang, W.K., 2001. Lovastatin-induced E2F-1 modulation and its effect on prostate cancer cell death. Carcinogenesis 22, 1727–1731.

Philipp-Staheli, J., Payne, S.R., Kemp, C.J., 2001. p27(Kip1): regulation and function of haploinsufficient tumour supressor and its misregulation in cancer. Exp. Cell Res. 264, 148–168.

Please, C.P., Pettet, G., McElwain, D.L.S., 1998. A new approach to modelling the formation of necrotic regions in tumours. Appl. Math. Lett. 11, 89–94.

Preziosi, L. (Ed.), 2003. Cancer Modelling and Simulation. CRC Press, Boca Raton, FL.

Pries, A.R., Secomb, T.W., Gessner, T., Sperandio, M.B., Gross, J.F., Gaehtgens, P., 1994. Resistance to blood flow in microvessels in vivo. Circ. Res. 75, 904–915.

Pries, A.R., Secomb, T.W., Gaehtgens, P., 1995. Design principles of vascular beds. Circ. Res. 77, 1017–1023.

Pries, A.R., Secomb, T.W., Gaehtgens, P., 1998. Structural adaptation and stability of microvascular networks: theory and simulations. Am. J. Physiol. 275, H349–H360.

Ribba, B., Marron, K., Agur, Z., Alarcón, T., Maini, P.K., 2003. Doxorubicin treatment efficiency on non-Hodgkin's lymphoma: computer model and simulation. Bull. Math. Biol., submitted for publication.

Rothman, D.H., Zalesky, S., 1997. Lattice-gas Cellular Automata: Simple Models of Complex Hydrodynamics. Cambridge University Press, Cambridge.

Royds, J.A., Dower, S.K., Qwarnstrom, E.E., Lewis, C.E., 1998. Response of tumour cells to hypoxia: role of p53 and NFkB. J. Clin. Pathol. Mol. Pathol. 51, 55–61.

Saito, J., 2001. Regulation of FRTL-5 thyroid cell growth by phosphatidylinositol (OH) 3 kinase-dependent Akt-mediated signaling. Thyroid 11, 339–351.

Stokke, T., Holte, H., Smedshammer, L., Smeland, E.B., Kaalhus, O., Steen, H.B., 1998. Proliferation and apoptosis in malignant and normal cells in B-cell non-Hodgkin's lymphomas. Br. J. Cancer 77, 1832–1838.

Turner, S., Sherrat, J.A., 2002. Intercellular adhesion and cancer invasion: a discrete simulation using the extended Potts model. J. Theor. Biol. 216, 85–100.

Tyson, J.J., Novak, B., 2001. Regulation of the eukariotic cell cycle: molecular antagonism, hysteresis, and irreversible transitions. J. Theor. Biol. 210, 249–263.

Ward, J.P., King, J.R., 1997. Mathematical modelling of avascular-tumour growth. IMA J. Math. Appl. Med. 14, 39–69.

Ward, J.P., King, J.R., 1999. Mathematical modelling of avascular-tumour growth II: modelling growth saturation. IMA J. Math. Appl. Med. 16, 171–211.

Yancopoulos, G.D., Davis, S., Gale, N.W., Rudge, J.S., Wiegand, S.J., Holash, J., 2000. Vascular specific growth factors and blood vessel formation. Nature 407, 242–248.